On dimensionless loading parameters for close-in blasts

Karl Micallef[a†], Arash Soleiman Fallah[b,*], Daniel J. Pope[c], Mojtaba Moatamedi[d], Luke A. Louca[e]

[a]Foster and Partners, Riverside, Hester Road, London, SW11 4AN, U.K.
[b]Department of Aeronautics, Roderic Hill Building, Imperial College London, London, SW7 2AZ, U.K.
[c]Physical Sciences Research Department, D.S.T.L., Porton Down, Salisbury, Wiltshire, SP4 0JQ, U.K.
[d]Centre for Nuclear Engineering, Department of Materials, Bessemer Building, Imperial College London, London SW7 2AZ, U.K.
[e]Department of Civil Engineering, Skempton Building, Imperial College London, London, SW7 2AZ, U.K.

ABSTRACT

Close-range blasts pose a threat through severe damage to structures and injury or death. In this work, the spatial and temporal descriptions of a localised blast load are presented using 6 non-dimensional parameters. These are found to be solely functions of the charge stand-off distance to diameter ratio for a cylindrically-shaped charge.

Numerical simulations of a localised blast are performed using AUTODYN, where the pressure variation on a rigid barrier for various charge stand-off/diameter combinations is obtained. The least-square regression is then utilised to obtain the relationship between stand-off/diameter ratio and dimensionless loading parameters. The relevant expressions and dimensionless charts are presented.

The proposed equations are verified by comparing experimental data with numerical results obtained by finite element analysis (FEA) of blast loaded steel plates (using the user-defined subroutine VDLOAD implemented in the FEA package ABAQUS/Explicit). Excellent correlation of the measured permanent displacement with numerically predicted results is obtained.

Keywords: Localised blast, non-dimensional parameters, AUTODYN, ABAQUS/Explicit

NOMENCLATURE

Latin upper case

A	explosive material constant [M L^{-1} T^{-2}]
B	explosive material constant [M L^{-1} T^{-2}]
C_p	gas specific heat at constant pressure, [L^2 T^{-2} θ^{-1}]
C_v	gas specific heat at constant volume, [L T^{-2} θ^{-1}]
D_e	diameter of explosive, [L]
E_0^e	specific energy of explosive, [L^2 T^{-2}]

*Corresponding Author: E-mail: as3@imperial.ac.uk

†Work was carried out as part of doctoral candidature at (e)

H	plate thickness, [L]
L	plate length, [L]
P	pressure, [M L^{-1} T^{-2}]
P_0	maximum overpressure, [M L^{-1} T^{-2}]
P_a	overpressure, [M L^{-1} T^{-2}]
$P(r, t)$	loading function, [M L^{-1} T^{-2}]
$P_s(r)$	spatial part of pressure pulse load, [M L^{-1} T^{-2}]
$P_t(t)$	temporal part of pressure pulse load, [M L^{-1} T^{-2}]
Q_e	energy of explosion, [L2 T^{-2}]
R_0	radius of central uniformly-loaded region, [L]
R_1	explosive material constant, [1]
R_2	explosive material constant, [1]
R_e	radius of explosive, [L]
T	gas temperature, [θ]
W	plate width, [L]

Latin lower case

b	loading parameter, [L^{-1}]
d	stand-off distance, [L]
f_i	functions of $\left(\frac{d}{D_e}\right)$, [1]
i	non-dimensional impulse, [1]
m_e	mass of explosive, [M]
r	radial axis direction, [L]
t_d	blast duration, [T]
w	loading parameter, [T^{-1}]
w_f	permanent transverse displacement, [L]

Greek upper case

Π_i	Buckingham's dimensionless groups, [1]

Greek lower case

λ	loaded radius ratio, [1]
λ_0	uniformly-loaded radius ratio, [1]
$\xi_{q.1}$	Jacob et al.'s loading parameter, [1]
$\xi_{q.S}$	Jacob et al.'s stand-off parameter, [1]
ρ	density of plate material, [M L^{-3}]
ρ_a	density of air, [M L^{-3}]
ρ_e	density of explosive, [M L^{-3}]
ρ_p	density of explosive product, [M L^{-3}]
$\phi_{q.S}$	Jacob et al.'s damage parameter for quadrangular plates with stand-off effect, [1]
σ_0	yield stress, [M L-1 T^{-2}]
ω	explosive material constant, [1]

1. INTRODUCTION

Proximal blasts cause particular threats to both human life and to civil and military infrastructure. The source of such blasts can be, for example, IEDs (improvised explosive devices) and buried land mines exploding onto the underside of military vehicles.

Many researchers (e.g. [1–5]) have studied the response of structures to global (or uniform) blast loading. However, when blasts occur in close proximity of engineering structures, the localised effect of the load gives rise to particular form of damage to the structure which requires particular consideration, different from those of the case of global blast loading [6].

1.1. LOCALISED BLAST LOADING

While there is no consensus on a unique universally accepted definition for "localised blast", researchers have proposed a few. Gharababaei et al. [7], for instance, define a localised blast load as one where the stand-off distance is less than the radius of a circular plate whereas Jacob et al. [8] attribute the localised nature to a blast load when the stand-off distance is less than the radius of the explosive charge. The main concern of the engineer falls, anyway, beyond the question of definition but the effects of such a load on engineering structures. In fact, various researchers have investigated the effect of localised blast on a variety of structural forms and material systems.

Florence [9, 10] and Conroy [11], to mention a few, provide analytical expressions describing the response of circular steel plates subjected to uniform localised loadings while Lee and Wierzbicki [12, 13] studied particular forms of failure in steel plates under localised blast loading. Qin [14] studied the response of sandwich and monolithic beams under localised impulsive loading.

In most engineering applications, structural elements can be geometrically classified as being either beams or plates. Beams are members whose lengths are large when compared to their (cross-sectional) sizes and whilst idealisation of frame structures into beam elements is justified, many engineering structures can be more readily idealised as being composed of plates. In fact, many researchers (e.g. [8, 15–18]) carried out considerable work related to localised blasts on steel plates, including the influence of stand-off on the response [8] and the effect of boundary conditions on plates subjected to localised blast loading [18].

Langdon et al. [19–25] have extensively studied localised blast loading on fibre-metal-laminates (FMLs), including studies on mathematical descriptions of a localised blast load [21].

1.2. NON-DIMENSIONALIZATION

Dimensionless parameters are a useful tool for scaling the effects of load and structural response also to avoid unnecessary repetition of, for example, experiments in the space of these dimensionless parameters.

Various researchers have used non-dimensional parameters to study elastic and plastic dynamic response of structures. An important number is Johnson's damage number [26], which describes the damage imparted by an impulsive velocity.

Zhao [27] and Li and Jones [28] extended Johnson's damage number to define a response number and applied it to various problems to define the response of plastic beams and plates loaded dynamically.

Li and Meng [29] developed dimensionless pressure-impulse diagrams which are pulse-shape independent for various elastic-plastic SDOF systems while Fallah and Louca [30] extended this work by considering hardening/softening responses.

However, dimensional analyses found in the literature typically deal with providing expressions for the dynamic response of structures subjected to given loading, rather than proposing expressions to describe the actual blast loading, given a set of threat parameters corresponding to a real case.

1.3. AIM OF CURRENT WORK

Given the aforementioned gap in the literature, the objective of the present study is to develop dimensionless expressions for a set of parameters which will define the variation of a localised blast, both spatially and temporally. These parameters are functions of a set of known loading inputs (viz. explosive type, charge mass, diameter and stand-off distance) which defined the problem uniquely. The study will be limited to centrally-detonated charges of a cylindrical shape whose height is relatively small when compared to its diameter. The dimensionless parameters are then used to define a loading distribution on a structure such that it can be easily input into commercial finite element packages for analysis. The results from the exercise are validated by comparison with experimental results from blast load tests on steel panels recently tested at the University of Cape Town.

2. NON-DIMENSIONALISED LOADING PARAMETERS

2.1. LOADING DESCRIPTION

In this work, it is assumed that a localised blast will be generated by means of a certain mass, m_e, of explosive material, having a heat of explosion, Q_e, having a shallow cylindrical form of diameter, D_e, and which is acting at a stand-off distance, d. Thus, the parameters which describe the load source are d, m_e, Q_e and D_e.

In general, an infinite series the terms of which are products of functions of space and time can express any loading function. In most works of the literature, the series has been truncated after the first term, and the localised blast loading function is assumed to be composed of 2 independent parts (as proposed in e.g. [15, 18, 21, 31]) as follows:

$$P(r, t) = P_s(r)\, P_t(t) \tag{1}$$

where $P_s(r)$ is the spatial distribution given by:

$$P_s(r) = \begin{cases} P_0, & 0 \le r \le R_0 \\ P_a e^{-br}, & r > R_0 \end{cases} \tag{2}$$

and $P_t(t)$ is the temporal distribution given by;

$$P_t(t) = \begin{cases} e^{-wt}, & 0 \le t \le t_d \\ 0, & t > t_d \end{cases} \tag{3}$$

In this work, t_d is the duration of the positive phase of the blast (assuming a zero rise time), P_0 is a value of constant pressure acting over a central circular region of radius R_0 and b and w are exponential decay factors describing the variation of the spatial and temporal functions respectively. Thus, the parameters which describe the loading profile completely are R_0, P_0, t_d, b and w.

It should be noted that P_a is not a further independent parameter, since P_a attaints the value of P_0 when the multiplier e^{-br} is evaluated at $r = R_0$.

The loading distribution is shown in Figure 1.

2.2. NON-DIMENSIONALIZATION

A non-dimensionalization exercise is carried out employing Buckingham's Π-theorem [32] and the following non-dimensional groups are extracted:

$$\prod_1 = \frac{P_0 t_d^{\,2} D_e}{m_e} \tag{4}$$

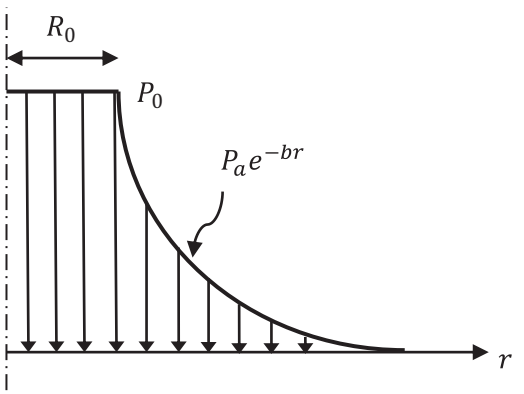

Figure 1: Load spatial distribution, P_s (r)

$$\prod_2 = \frac{Q_e t_d^{\,2}}{D_e^{\,2}} \tag{5}$$

$$\prod_3 = \frac{R_0}{D_e} \tag{6}$$

$$\prod_4 = D_e b \tag{7}$$

$$\prod_5 = w t_d \tag{8}$$

$$\prod_6 = \frac{d}{D_e} \tag{9}$$

Through some algebraic manipulation, is it found that the 5 unknown parameters R_0, P_0, t_d, a, b and w are all functions of $\left(\frac{d}{D_e}\right)$ as follows:

$$P_0 = \frac{Q_e m_e}{D_e^{\,3}} \left\{ f_1\left(\frac{d}{D_e}\right) \right\} \tag{10}$$

$$t_d = \frac{D_e}{\sqrt{Q_e}} \left\{ f_2\left(\frac{d}{D_e}\right) \right\} \tag{11}$$

$$w = \frac{\sqrt{Q_e}}{D_e} \left\{ f_3\left(\frac{d}{D_e}\right) \right\} \tag{12}$$

$$R_0 = D_e \left\{ f_4\left(\frac{d}{D_e}\right) \right\} \tag{13}$$

$$b = \frac{1}{D_e} \left\{ f_5\left(\frac{d}{D_e}\right) \right\} \tag{14}$$

The ratio $\left(\frac{d}{D_e}\right)$ in this case can be compared with and shown to be related to the traditional scaled distance expressed in the Hopkinson [33] and Cranz [34] scaling law, i.e., $\left(\frac{d}{m_e^{\frac{1}{3}}}\right)$.However, this the ratio$\left(\frac{d}{D_e}\right)$, being dimensionless and derived solely based on Buckingham's Π-theorem without any empirical knowledge of blast phenomena, can be thought of as a more theoretically sound scaling parameter than the Hopkinson-Cranz scaled distance, since the dimensional analysis proposed in this work will also enable the derivation of the spatial and temporal decaying functions describing the blast load.

The remaining task would thus be, to establish the functional dependence i.e. the form of the functions $f_i\left(\frac{d}{D_e}\right)$ in equations (10) to (14).

3. PARAMETRIC STUDIES USING AUTODYN

For the purpose of this study, the range of $\left(\frac{d}{D_e}\right)$ being considered is within the interval $0.5 \leq \left(\frac{d}{D_e}\right) \leq 6$, which is deemed to be representative of practical loading scenarios which can be described as being "localised". This would correspond to threats placed at stand-off distances in the range of 400 to 500 mm from IEDs of a range of diameters from 50 to 800 mm.

A set of 12 models was compiled using AUTODYN v.13.0 [35], a hydrocode specifically designed for non-linear dynamic analysis and routinely use to simulate blast loadings. A 2D axially-symmetric model was set up representing a cylindrical space of 300 mm diameter and 500 mm height and meshed uniformly with an Eulerian mesh of uniform 1 mm size, which was found to ensure numerical convergence.

Flow-out boundary conditions were assigned to the curved face and the top (flat) face of the cylindrical space while the other flat face was modelled as a rigid boundary.

3.1. AIR MODELLING

The space was filled with air using material data from the AUTODYN material library using an "ideal gas" equation of state, described by:

$$P = \rho_a \left(\frac{C_p}{C_v} - 1\right) C_v T \tag{15}$$

where P is the gas pressure, ρ_a = 1.225 kg/m^3 is the density of air, C_p = 1.005 kJ/kgK is the specific heat at constant pressure, C_v = 0.7176 kJ/kgK is the specific heat at constant volume and T = 288.2 K is the gas temperature. The internal energy was assigned as 2.068E5 kJ/kg.

3.2. EXPLOSIVE MODELLING

The explosive charge was modelled as a 10 mm high cylindrical block of C4 (PE4) explosive of constant diameter, D_e, of 50 mm and constant mass, m_e, of 31.4g. A detonation point was placed in the centroid of the cylindrical charge.

The Jones-Wilkins-Lee (JWL) equation of state was used to describe the explosive's detonation behaviour:

$$P = A\left(1-\frac{\omega\rho_p}{R_1\rho_e}\right)e^{-\frac{R_1\rho_e}{\rho_p}} + B\left(1-\frac{\omega\rho_p}{R_2\rho_e}\right)e^{-\frac{R_2\rho_e}{\rho_p}} + \omega\rho_e E_0^e \tag{16}$$

where P is the pressure, ρ_e = 1601 kg/m^3 is the density of the explosive, ρ_p is the density of the explosive product, E_0^e = 5.621488E6 kJ/kg is the explosive's specific internal energy and A = 609.77 GPa, B = 12.95 GPa, R_1 = 4.5, R_2 = 1.4 and ω = 0.25 are empirically-derived material constants.

3.3. MODELLING RESULTS

In each of the models, the stand-off distance was varied, from 25 mm to 300 mm in 25 mm increments. In each case, the pressure value on the rigid face was monitored at 60 gauge points placed at 5 mm intervals, as shown in Figure 2.

In each case, the detonation was numerically simulated and the event was modelled up to 2 ms, monitoring the pressure in the domain (e.g. Figure 3 to Figure 5) at the gauge points.

From each of the gauge points, the pressure-time histories were obtained. A selection of these results from one of the models is shown in Figure 6.

For each model, the variation of pressure with space and time could be established, assuming the relationships in (2) and (3). The curve fitting was done using built-in curve fitting tool in MATLAB [36] and the parameters R_0, P_0, t_d, b and w were extracted. An example of the fits is shown in Figure 7 and Figure 8.

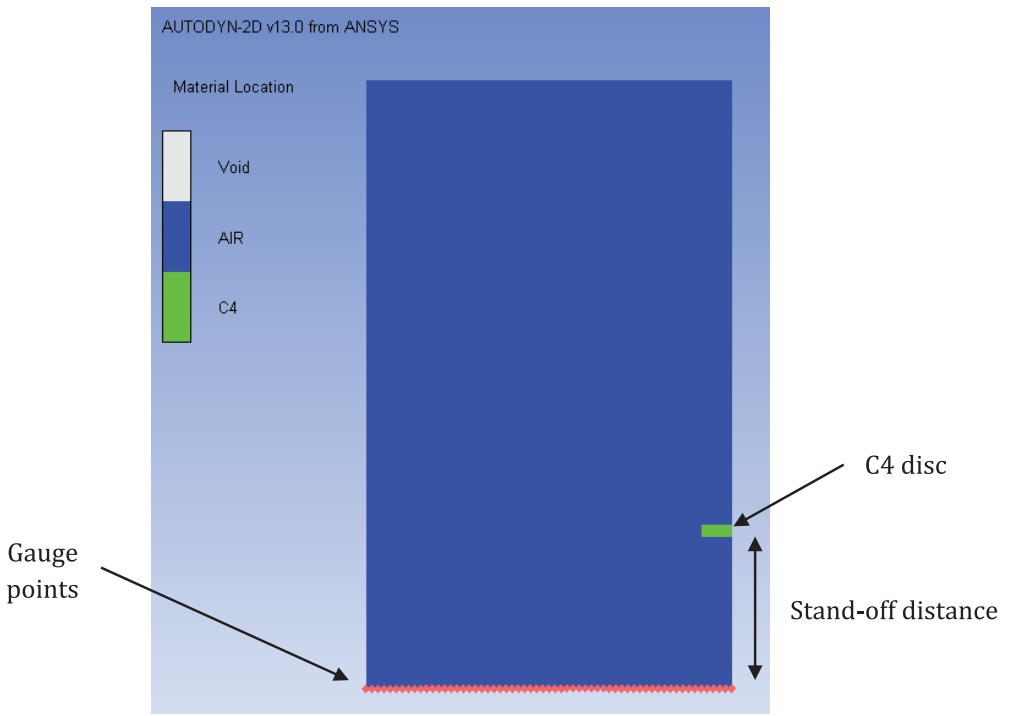

Figure 2: AUTODYN model setup

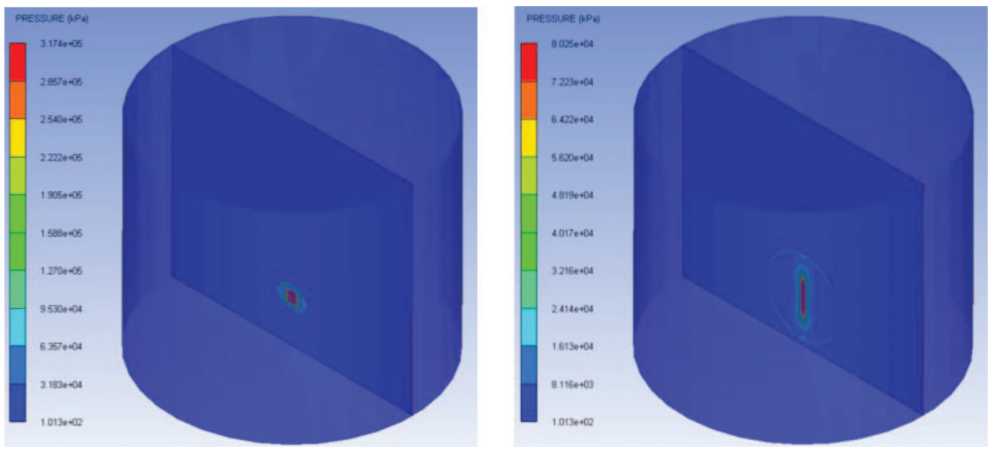

Figure 3: Pressure distribution for 100 mm stand-off (left: 0.01 ms, right: 0.02 ms)

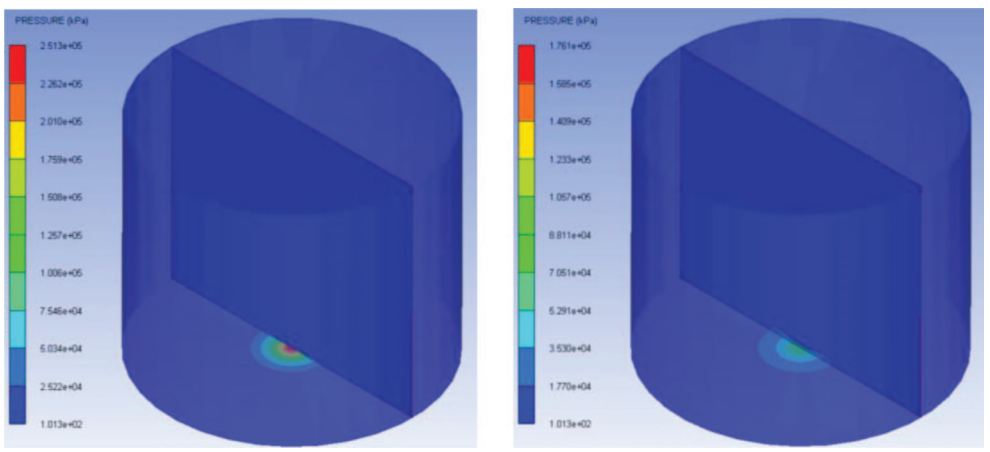

Figure 4: Pressure distribution for 100 mm stand-off (left: 0.03 ms, right: 0.04 ms)

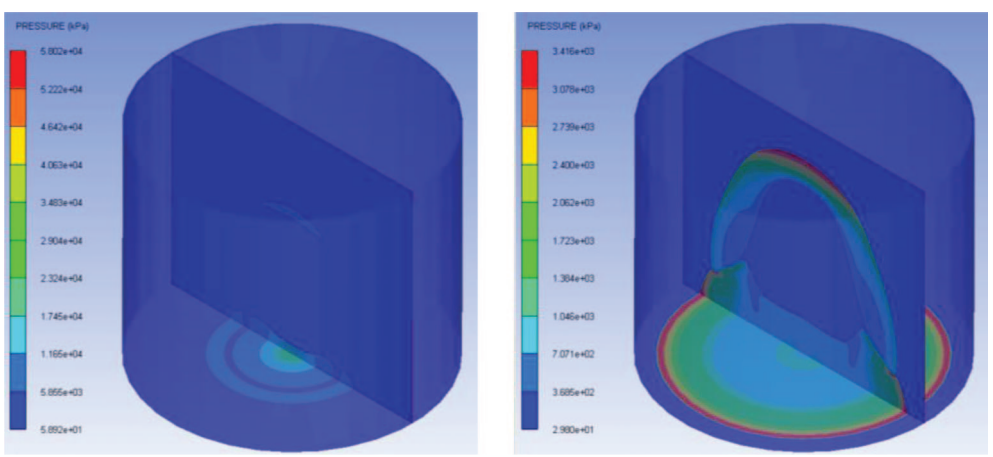

Figure 5: Pressure distribution for 100 mm stand-off (left: 0.05 ms, right: 0.1 ms)

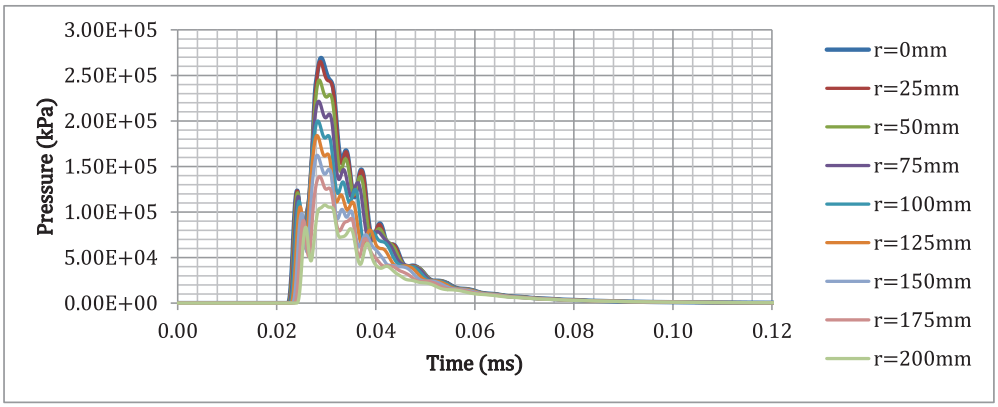

Figure 6: Pressure-time history for 100 mm stand-off

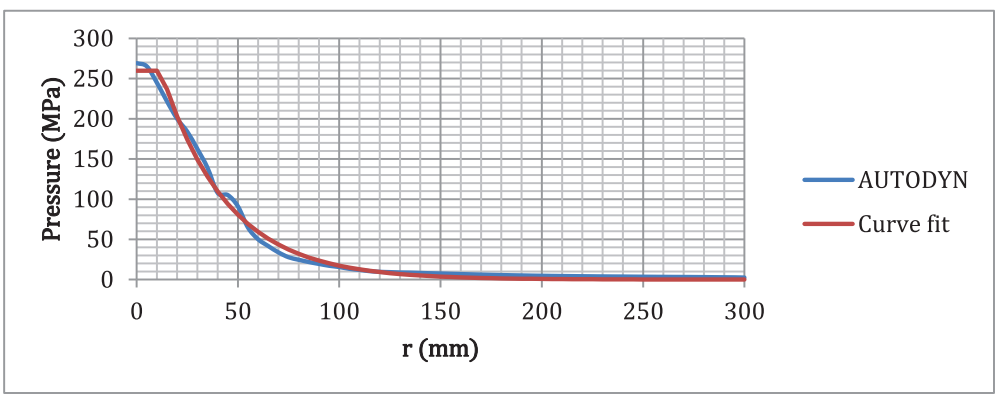

Figure 7: Spatial load variation for 100 mm stand-off

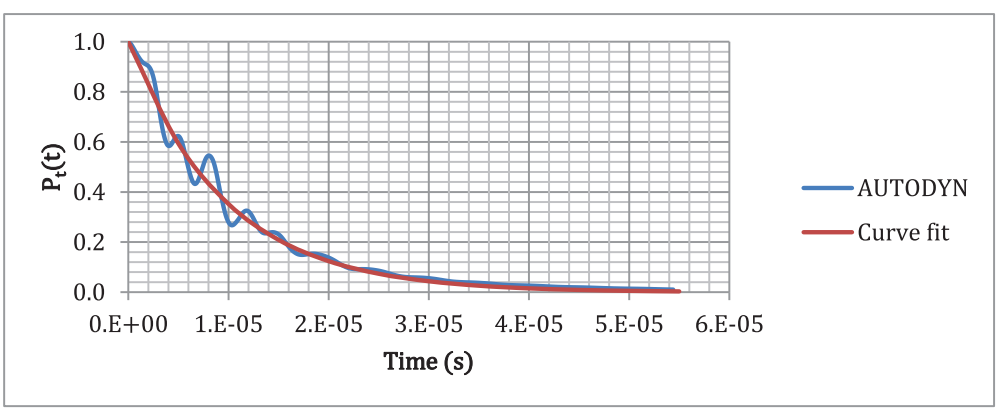

Figure 8: Temporal load variation for 100 mm stand-off

4. LOADING PROFILE EQUATIONS AND CHARTS

Using the results obtained during the process outline in Section 3, a series of least-square fitting exercises were carried out using the built-in curve fitting tool in MATLAB [36].

Thus, the functions f_i in equations (10) to (14) were established as follows:

$$f_1 = (0.4994)\left(\frac{d}{D_e}\right)^{-1.391} \tag{17}$$

$$F_2 = \begin{cases} 6.055\ e^{-2.17\left(\frac{d}{D_e}\right)} + 2.389\ e^{-0.03591\left(\frac{d}{D_e}\right)}, & 0 \le \left(\frac{d}{D_e}\right) \le 3.5 \\ -1.76\left(\frac{d}{D_e}\right) + 8.25, & 3.5 \le \left(\frac{d}{D_e}\right) \le 4.0 \\ -0.226\left(\frac{d}{D_e}\right) + 2.136, & 4.0 \le \left(\frac{d}{D_e}\right) \le 6.0 \end{cases} \tag{18}$$

$$f_3 = (0.9114)e^{0.4418\left(\frac{d}{D_e}\right)} \tag{19}$$

$$f_4 = \begin{cases} -0.07\left(\frac{d}{D_e}\right) + 0.375, & 0 \le \left(\frac{d}{D_e}\right) \le 2.0 \\ 0.2547\left(\frac{d}{D_e}\right) - 0.2542, & 2.0 \le \left(\frac{d}{D_e}\right) \le 6.0 \end{cases} \tag{20}$$

$$f_5 = (2.528)\left(\frac{d}{D_e}\right)^{-0.7119} \tag{21}$$

These are shown graphically in Figure 9 to Figure 13.

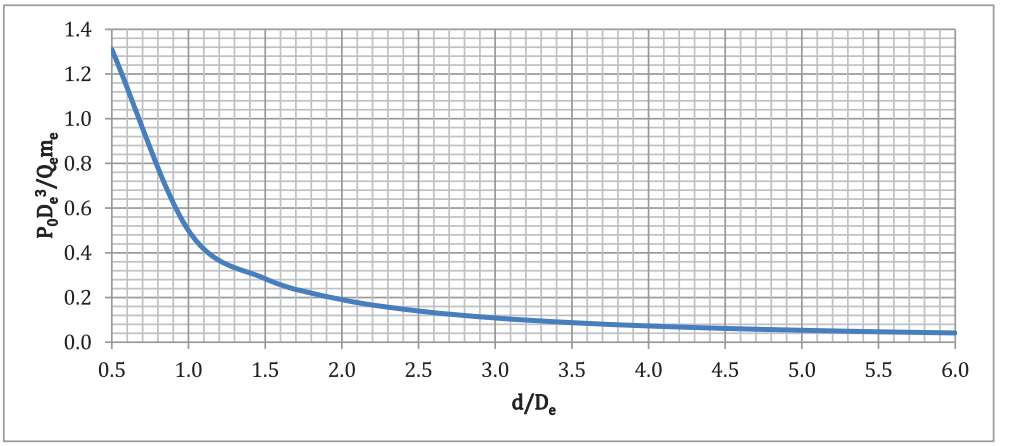

Figure 9: Non-dimensionalized constant pressure

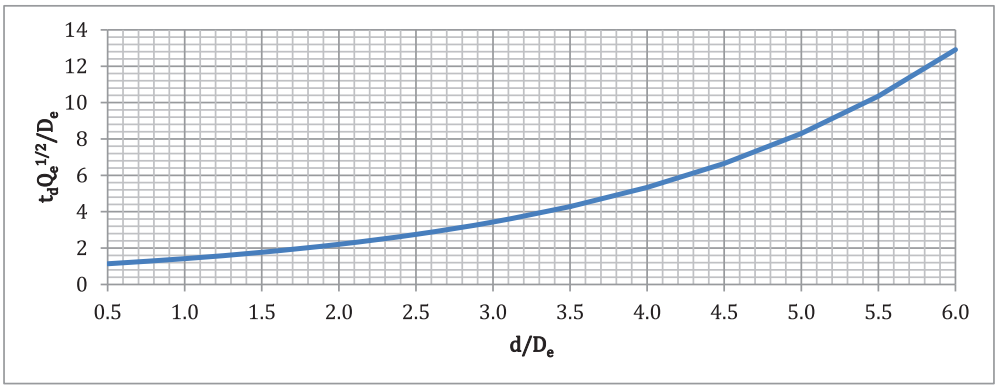

Figure 10: Non-dimensionalized duration

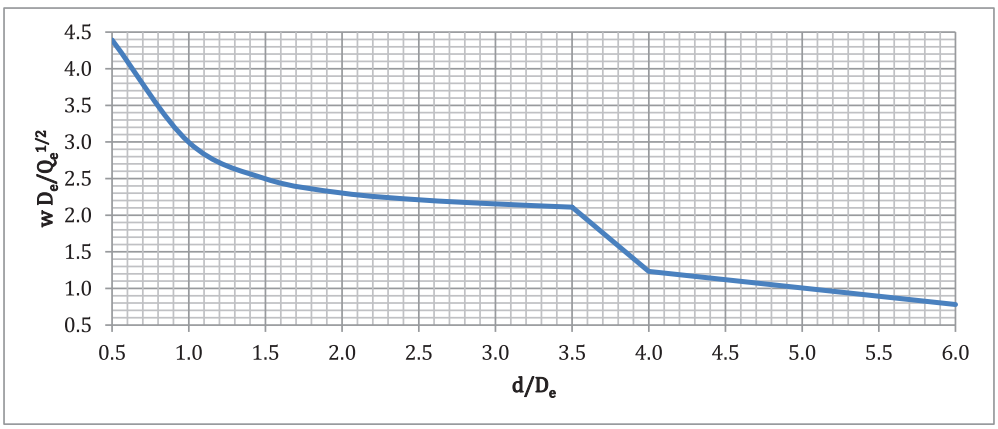

Figure 11: Non-dimensionalized temporal decay factor

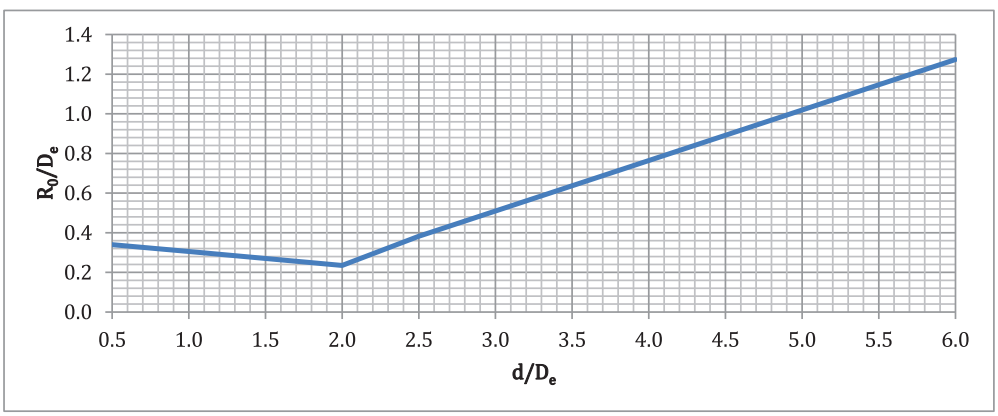

Figure 12: Non-dimensionalized constant pressure radius

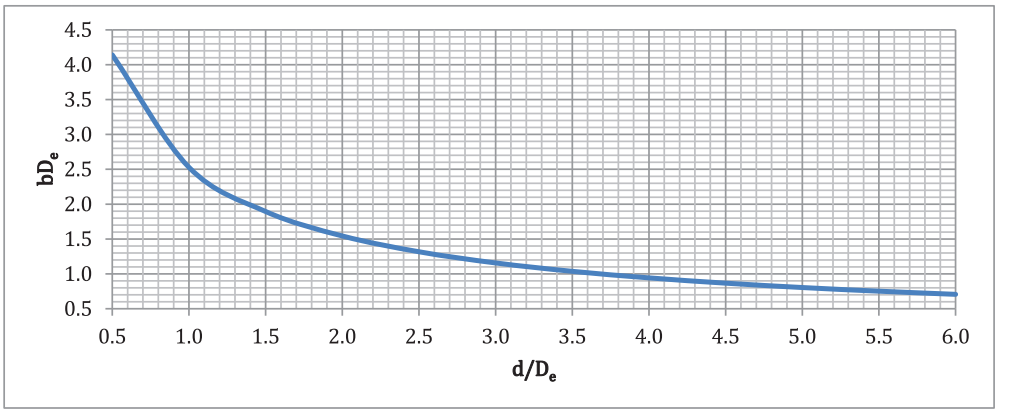

Figure 13: Non-dimensionalized spatial decay factor

5. VARIATION OF IMPULSE WITH LOADING

Having established the form of the loading (spatial and temporal) distributions, a discussion on the variation of impulse with the various loading parameters is presented hereunder.

From (1) and using (2) and (3), an expression for the impulse in terms of the loading radius r could be written as:

$$I(r) = 2\pi \int_0^{t_d} \int_0^{r} P\left(r^*, t^*\right) r^* dr^* dt^* \tag{22}$$

Considering a target of radius R and defining the ratio $\lambda = \frac{r}{R}$ and $\lambda_0 = \frac{R_0}{R}$ and substituting in (22), then $I(\lambda)$ could be written as:

$$I(\lambda) = \begin{cases} \dfrac{\pi P_0 \left(1 - e^{-wt_d}\right)\left(\lambda_0 R\right)^2}{w}, & \lambda < \lambda_0 \\ \dfrac{\pi P_0 \left(1 - e^{-wt_d}\right)}{w}\left(\left(\lambda_0 R\right)^2 + \dfrac{2e^{-\lambda_0 Rb}}{b^2}\left\{e^{-\lambda_0 Rb}\left[1 + \lambda_0 Rb\right] - e^{-b\lambda R}\left[1 + \lambda Rb\right]\right\}\right), & \lambda \geq \lambda_0 \end{cases} \tag{23}$$

The total impulse which a given charge could potentially deliver to the target would be given by:

$$I(\infty) = \lim_{\lambda \to \infty}\left\{I(\lambda)\right\} = \frac{\pi P_0 \left(1 - e^{-wt_d}\right)\left(\lambda_0 R\right)^2}{w} + \frac{2\pi\left(1 - e^{-wt_d}\right) P_0 \left(1 + \lambda_0 Rb\right)}{wb^2} \tag{24}$$

Thus, a non-dimensional impulse, i, could be defined as the ratio of the impulse imparted to a target to the total impulse which the threat generates:

$$i = \frac{I(\lambda)}{I(\infty)} = \begin{cases} \dfrac{\left(\lambda_0 Rb\right)^2}{2 + 2\lambda_0 Rb + \left(\lambda_0 Rb\right)^2}, & \lambda < \lambda_0 \\ \dfrac{2 + 2\lambda_0 Rb + \left(\lambda_0 Rb\right)^2 - 2e^{-Rb\left(\lambda - \lambda_0\right)}\left[1 + \lambda Rb\right]}{2 + 2\lambda_0 Rb + \left(\lambda_0 Rb\right)^2}, & \lambda \geq \lambda_0 \end{cases} \tag{25}$$

The variation of i with λ for $\lambda \geq \lambda_0$ (which is the typical case in most practical applications) for various values of $\left(\frac{D_e}{R}\right)$ at different values of $\left(\frac{d}{D_e}\right)$ is shown graphically in Figure 14 to Figure 17.

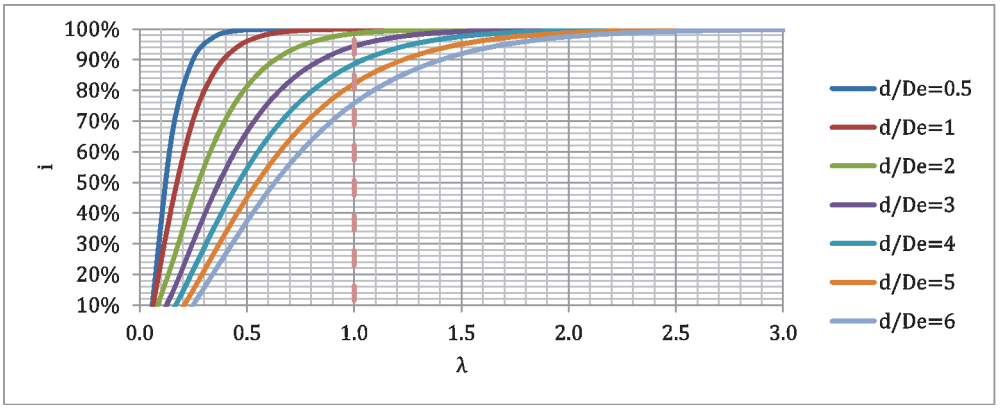

Figure 14: Variation of i with λ for $D_e/R = 0.25$

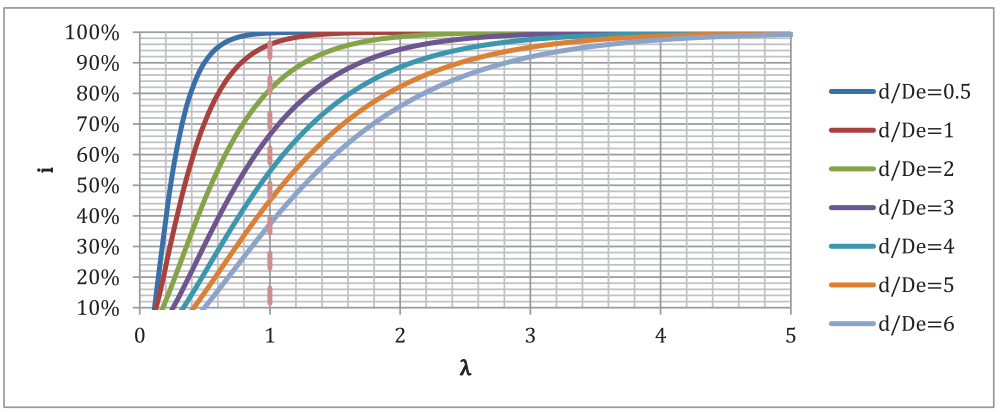

Figure 15: Variation of i with λ for $D_e/R = 0.5$

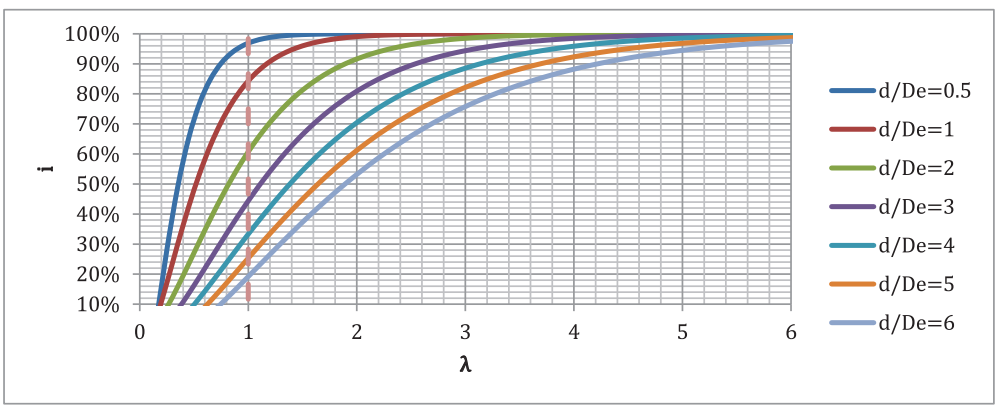

Figure 16: Variation of i with λ for $D_e/R = 0.75$

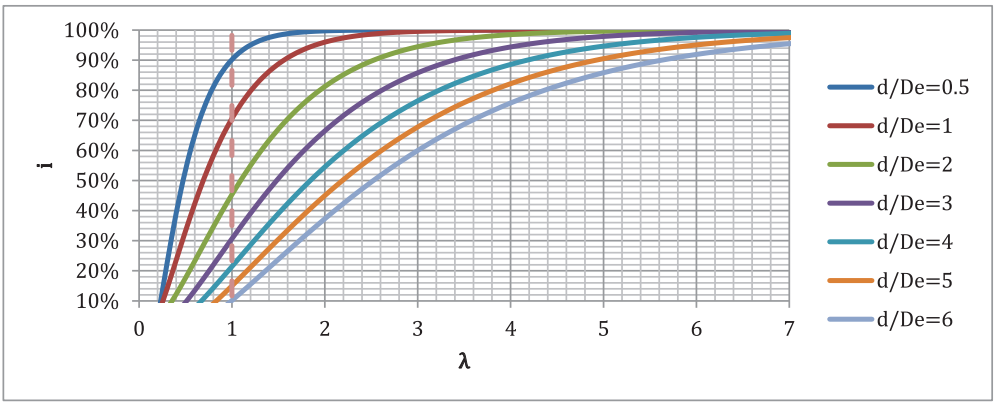

Figure 17: Variation of i with λ for $D_e/R = 1$

It can be observed that, as $\left(\frac{D_e}{R}\right)$ increases, then for a given stand-off to charge diameter ratio, i.e., $\left(\frac{d}{D_e}\right)$, the impulse imparted to the target decreases. Thus, it can be concluded that the more significant threat scenario would be a small stand-off to charge diameter ratio, rather than a large charge diameter to plate diameter ratio.

It can also be seen that, for low values of $\left(\frac{D_e}{R}\right)$, there is little reduction in impulse imparted with increasing charge stand-off and the amount of impulse imparted is reasonably high even for distant charges (e.g. for $\left(\frac{D_e}{R}\right) = 0.25, i = 75\%$ for $\left(\frac{d}{D_e}\right) = 6$). Thus, it can also be concluded that a threat scenario comprising small charge diameter to target radius ratio would be significantly detrimental to the target even for large stand-off to charge diameter ratios.

6. CORRELATION OF NUMERICAL WITH EXPERIMENTAL DATA

The results derived in Section 4 were verified by comparing experimental test data with numerical results which utilize the proposed model parameters.

6.1. TEST SETUP AND RESULTS

Laboratory testing of localised blast loading on steel plates was carried out at the Blast and Impact Survivability Research Unit within the University of Cape Town in South Africa using the ballistic pendulum setup therein (refer to e.g. [37] for details of setup). 3.8 mm thick Armox 370T Class 1 armour steel sourced from SSAB of Sweden [38] fully-clamped panels with an exposed area of 300 × 300 mm were subjected to a centrally-located disc of PE4 (or C4) explosive, which was mounted on a polystyrene bridge to give a desired stand-off distance. This arrangement has a long history of successful use and application of laboratory-scale blasts tests on metallic (e.g. [15, 39–41]) and also composite and hybrid

systems (e.g. [19, 21, 25, 31, 37]). Whilst in the past solid polystyrene blocks have been utilized as spacers to obtain a required stand-off, in this set of experiments a bridge arrangement has been used, shown in Figure 18. In this way, the polystyrene does not interfere with the overall blast phenomenon and there is no undesired enhancement of the blast effects to a specific area.

The tests are summarized in Table 1 and Figure 20.

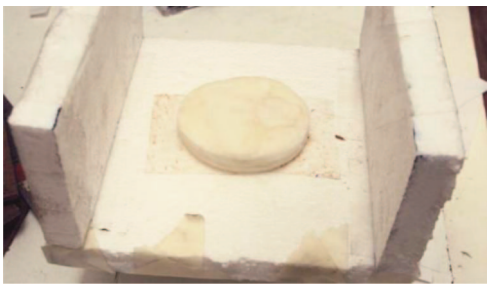

Figure 18: PE4 charge on underside of polystyrene bridge

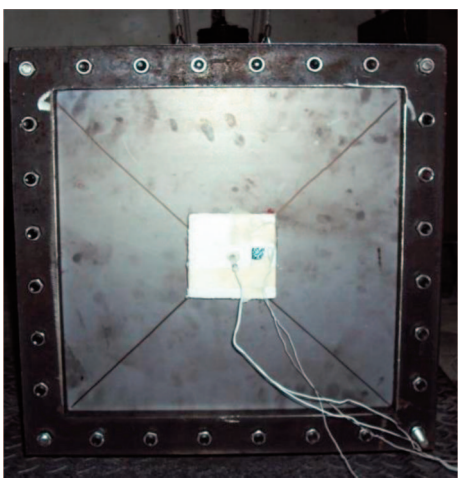

Figure 19: Typical test panel in position

Table 1: Test results for Armox 370T Class 1

Test	d **(mm)**	D_e **(mm)**	m_e **(g)**	I **(Ns)**[†]	w_f **(mm)**
1	25	50	40	80.0	29.5
2	25	50	33	66.1	21.9
3	50	50	40	82.2	14.4
4	50	50	70	143.2	25.6
5	38	50	40	100.1	21.3
6	38	50	50	80.5	27.1
7	38	40	40	82.2	17.6
8	38	40	50	91.0	18.6

[†]Measured by means of ballistic pendulum at the University of Cape Town.

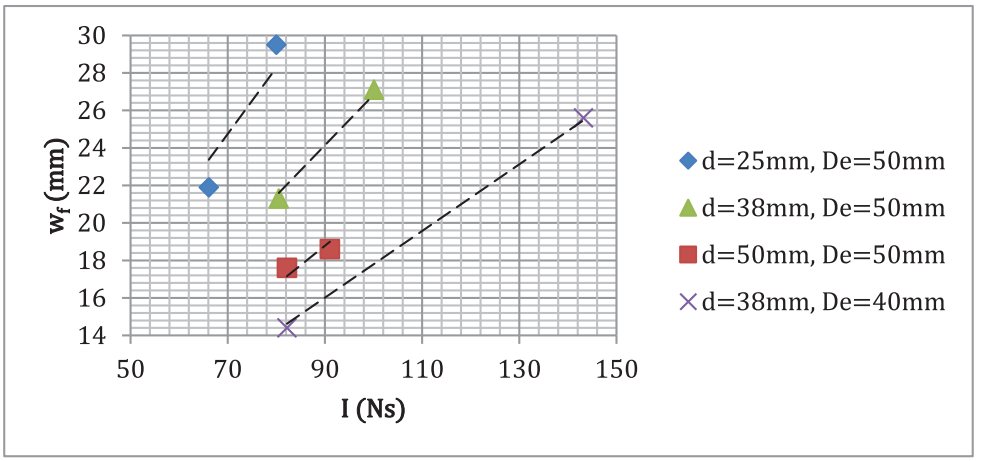

Figure 20: Variation of permanent displacement with impulse for Armox 370T Class 1

These results confirm the conclusions drawn from the theoretical analysis of Section 5, since, for both materials, it can be observed that, for the same D_e value, the permanent displacement is smaller as d increases and, for the same level of impulse and at a given stand-off distance, the permanent displacement is higher for larger values of D_e.

However, in terms of the variation of permanent displacement with impulse, it was observed there is a strong dependence on $\left(\frac{d}{D_e}\right)$, as evident from Figure 20.

6.2. DIMENSIONLESS RESULTS

Using the dimensionless damage number (or dimensionless impulse), $\phi_{q,S}$, proposed by Jacob et al. [8], this dependency is accounted for by means of a stand-off distance parameter for quadrangular plates of dimensions L and W, thickness H, static yield stress σ_0 and density ρ, subjected to an impulse I resulting from a charge of radius R_e, given by [16]:

$$\phi_{q,S} = \frac{I}{2H^2\sqrt{LW\rho\sigma_0}}\left(\frac{\xi_l}{\xi_S}\right) \tag{26}$$

where ξ_l is a loading parameter given by:

$$\xi_l = 1 + ln\left(\frac{LW}{\pi R_e^2}\right) \tag{27}$$

and ξ_S is a stand-off distance parameter given by:

$$\xi_S = 1 + ln\left(\frac{d}{R_e}\right) \tag{28}$$

The experimental results are now shown in terms of dimensionless quantities in Figure 21.

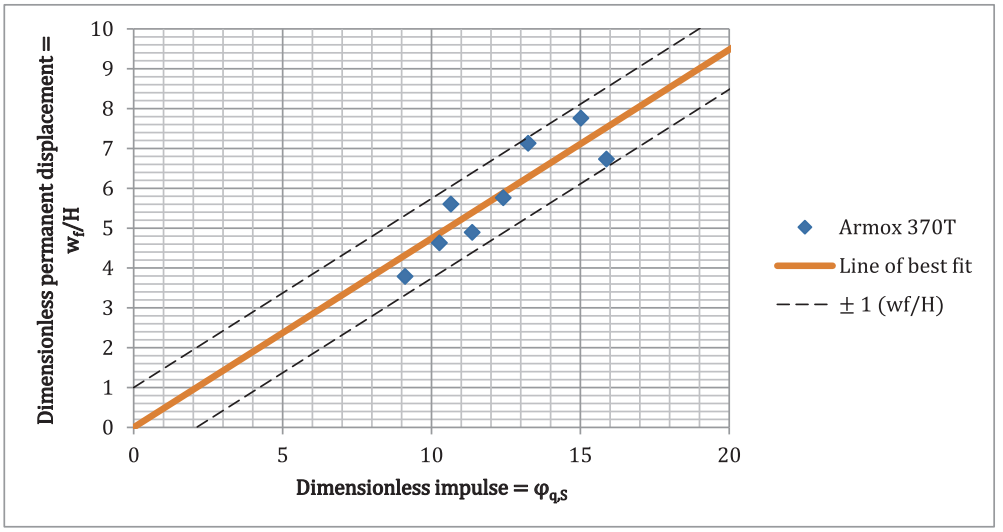

Figure 21: Variation of dimensionless displacement with dimensionless impulse

It can be observed that all results, stand-off distance and charge diameter, can be described by a single linear function which can be obtained by a least-squares fit analysis, falling within a displacement/thickness ratio of ±1, given by:

$$\left(\frac{w_f}{H}\right) = 0.474\ \phi_{q,S} \tag{29}$$

6.3. NUMERICAL RESULTS

Having obtained a set of experimental data, the test scenarios were modelled in a commercial finite element analysis package, defining the blast load by means of the function proposed in (1) to (3).

For the various d, D_e and m_e values described in Table 1, the loading parameter values were obtained from Figure 9 to Figure 13 or from equations (17) to (21). These loading distributions were implemented in a user-defined loading subroutine (VDLOAD) in the commercial finite element analysis package ABAQUS/Explicit v.6.9-1 [42] and applied onto the plate surface.

The plate itself was modelled using 8-noded linear brick elements with reduced integration and hourglass control (C3D8R). Due to symmetry, a quarter plate was modelled for computational efficiency and a uniform mesh size of 3 mm was used. This was established by ensuring that there is numerical convergence and that the artificial (hourglass) energy does not exceed ≈5% of the internal energy of the system. A typical comparison of the energy levels, which is representative of all the numerical models, is shown in Figure 22.

In terms of the material model, an elasto-plastic model was used for the armour steel, using the elastic properties of an initial modulus of 202.5 GPa and a Poisson's ratio of 0.33 and the plastic behaviour defined by using (true) stress-strain data obtained from tensile

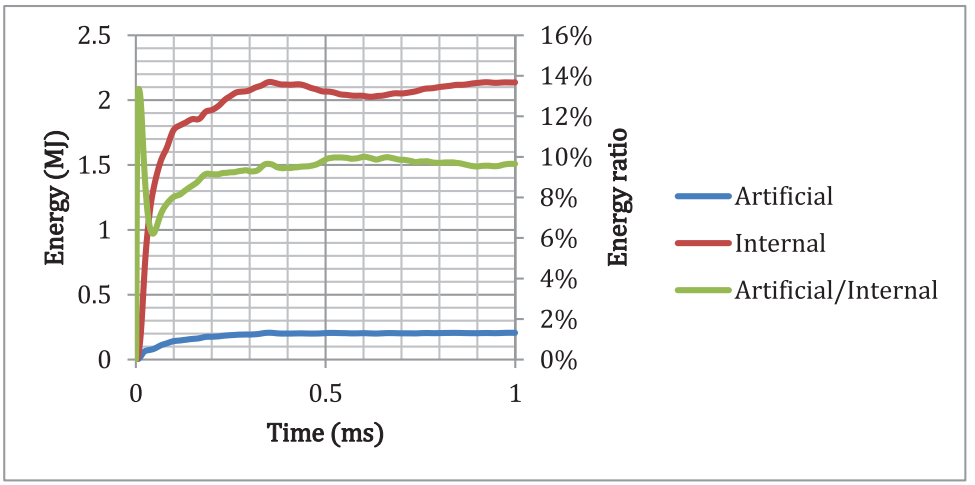

Figure 22: Energy comparison from ABAQUS (test 2)

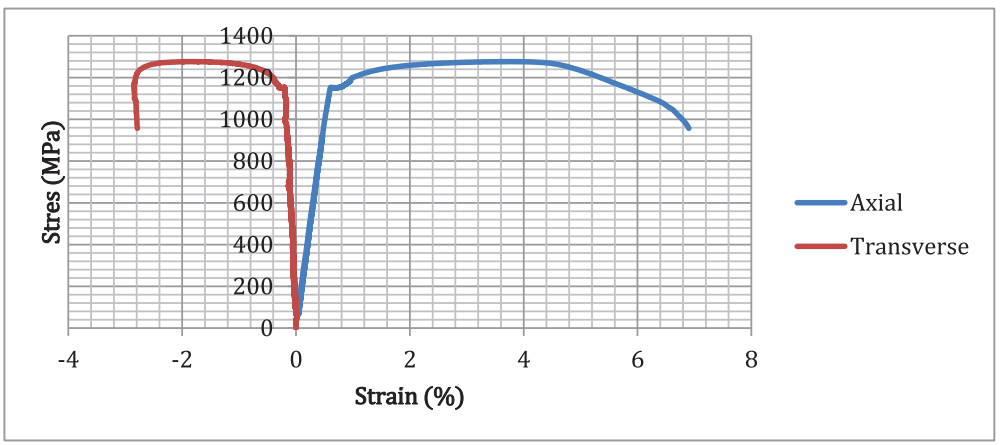

Figure 23: Stress-strain curve for Armox 370T Class 1

testing carried out at the Department of Civil and Environmental Engineering of Imperial College London, as shown in Figure 23.

A selection of the outputs from ABAQUS is shown in Figure 24 and Figure 25 and the results are summarised in Table 2.

It can be seen that there is good correlation between the experimental and numerical results, with a maximum difference of 11.9% and a mean difference of 8%.

In addition to loading uncertainties, the discrepancy can be attributed to the simplifications associated with the material model (i.e. ignoring rate effects) and also due to difference in support conditions, i.e., between the (fully-clamped) model and the (bolted) test plate.

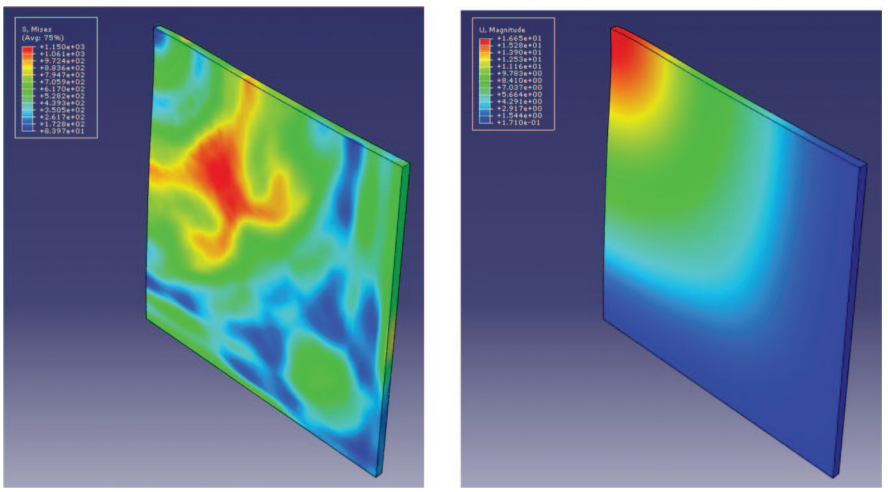

Figure 24: Mises stress (left) and displacement (right) contour plots for test 3

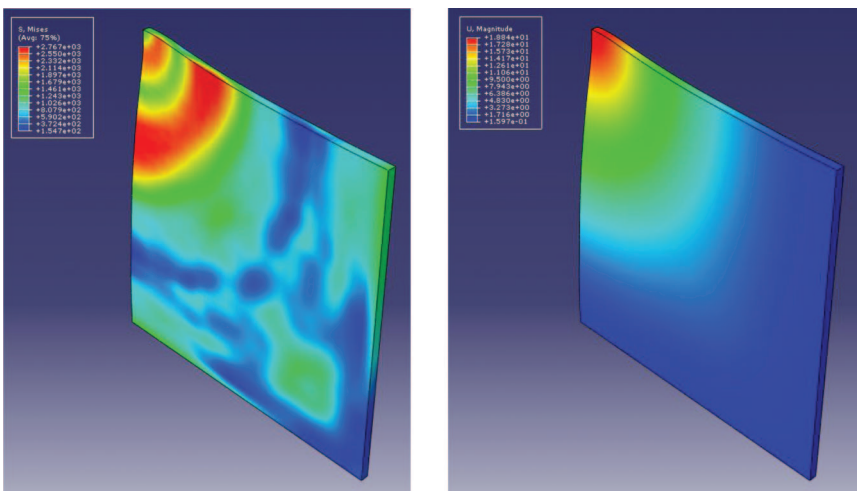

Figure 25: Mises stress (left) and displacement (right) contour plots for test 7

Table 2: Comparison between experimental and numerical results

Test	w_f (mm)	
	Experimental	**Numerical**
1	29.5	26.0
2	21.9	20.5
3	14.4	13.0
4	25.6	23.0
5	21.3	18.0
6	27.1	25.5
7	17.6	19.0
8	18.6	23.5

7. DISCUSSION AND CONCLUSIONS

In this work, a generalized form of spatial and temporal description of a localised blast load is presented. It is postulated that the two parts (spatial and temporal) are independent, an assumption supported by AUTODYN simulations. Assuming that the explosive charge is cylindrical in shape and that its height is not too large when compared to its diameter, a non-dimensionalization exercise is carried out, through which 6 dimensionless parameters which uniquely describe the load are extracted. These are all found to be a function of the ratio of the charge stand-off distance to the charge diameter.

A number of numerical simulations using AUTODYN were carried out, in which the pressure variation on a rigid barrier for various charge stand-off/diameter ratio combinations and the temporal and spatial variations are obtained for each case.

It should be noted that the relationships are obtained based on the assumption that the load is applied on a rigid barrier and ignoring the flexibility of the loaded structure. In effect, the structure would deform as it is loaded, making the results obtained through this method an upper bound to the exact solution. The accuracy of the method, nonetheless, is tested via corroboration of test results with subsequent simulations.

Least-square regression is performed to obtain the relationship between stand-off/diameter ratio and the various loading parameters and dimensionless charts for each of these parameters are produced.

The proposed method is verified by comparing experimental data with numerical models of a blast load on steel plates using ABAQUS/Explicit and modelling the load via a user-defined loading subroutine (VDLOAD) and utilizing the loading parameters obtained from the charts.

From the results obtained in Section 6.3, it is clear that the proposed method accurately describes localised blast loads and can be used to simulate the response of structures in finite element packages, such as ABAQUS/Explicit, and also to obtain analytical results using exact solutions where these exist. The proposed and investigated model was further used to study numerous similar cases and led to successful results in each case [43–46].

A final remark on the generality of the proposed method seems in order. It must be noted that while the proposed method can be applied for alternative charge geometries (e.g. spherical), the derived constants are only valid for cylindrical charges with a detonation point placed in the centre of the charge and where the cylinder's height is small when compared to its diameter (not exceeding 0.3). It is known that the influence of the charge height to its diameter could influence the spatial distribution and pressure magnitudes of a close-in blast and any scenarios outside those considered in this study would need further investigation.

ACKNOWLEDGEMENTS

This work is part of a project jointly funded by DSTL/MoD and EPSRC of the UK (EP/G042861/1).

REFERENCES

[1] Baker, W. E., Kulesz, J. J., Richer, R. E., Bessey, R. L. and Westine, P. S., Parr, V. B., *Workbook for predicting pressure wave and fragment effect of exploding propellent tanks and gas storage vessels*, 1975, NASA.

[2] Baker, W. E., Westine, P. S., Kulesz, J. J., Wilbeck, J. S. and Cox, P. A., *A manual for the prediction of blast and fragment loadings on structures*, 1980: Amarillo, Texas.

[3] Ginsburg, S. and U. Kirsch, Design of protective structures against blast. *Journal of Structural Engineering*, 1983. 109(6): p. 1490–1506.

[4] Boh, J. W., L. A. Louca and Y. S. Choo, Energy absorbing passive impact barrier for profiled blastwalls. *International Journal of Impact Engineering*, 2005. 31(8): p. 976–995.

[5] Louca, L. A. and R. M. Mohamed Ali, Improving the ductile behaviour of offshore topside structures under extreme loads. *Engineering Structures*, 2008. 30(2): p. 506–521.

[6] Rajendran, R. and J. M. Lee, Blast loaded plates. *Marine Structures*, 2009. 22(2): p. 99–127.

[7] Gharababaei, H. and A. Darvizeh, Experimental and analytical investigation of large deformation of thin circular plates subjected to localised and uniform impulsive loading. *Mechanics Based Design of Structures and Machines*, 2010. 38(2): p. 171–189.

[8] Jacob, N., G. N. Nurick and G. S. Langdon, The effect of stand-off distance on the failure of fully clamped circular mild steel plates subjected to blast loads. *Engineering Structures*, 2007. 29(10): p. 2723–2736.

[9] Florence, A. L., Clamped circular rigid-plastic plates under central blast loading. *International Journal of Solids and Structures*, 1966. 2(2): p. 319–335.

[10] Florence, A. L., Response of circular plates to central pulse loading. *International Journal of Solids and Structures,* 1977. 13(11): p. 1091–1102.

[11] Conroy, M. F., Rigid-plastic analysis of a simply supported circular plate due to dynamic circular loading. *Journal of the Franklin Institute*, 1969. 288(2): p. 131–135.

[12] Lee, Y. -W. and T. Wierzbicki, Fracture prediction of thin plates under localised impulsive loading. Part I: dishing. *International Journal of Impact Engineering*, 2005. 31(10): p. 1253–1276.

[13] Lee, Y. -W. and T. Wierzbicki, Fracture prediction of thin plates under localised impulsive loading. Part II: discing and petalling. *International Journal of Impact Engineering*, 2005. 31(10): p. 1277–1308.

[14] Qin, Q. H., T. J. Wang and S. Z. Zhao, Large deflections of metallic sandwich and monolithic beams under locally impulsive loading. *International Journal of Mechanical Sciences*, 2009. 51(11–12): p. 752–773.

[15] Langdon, G. S., S. C. K. Yuen and G. N. Nurick, Experimental and numerical studies on the response of quadrangular stiffened plates. Part II: localised blast loading. *International Journal of Impact Engineering*, 2005. 31(1): p. 85–111.

[16] Jacob, N., et al., Scaling aspects of quadrangular plates subjected to localised blast loads - experiments and predictions. *International Journal of Impact Engineering*, 2004. 30(8-9): p. 1179–1208.

[17] Wierzbicki, T. and G. N. Nurick, Large deformation of thin plates under localised impulsive loading. *International Journal of Impact Engineering*, 1996. 18(7–8): p. 899–918.

[18] Bonorchis, D. and G. N. Nurick, The influence of boundary conditions on the loading of rectangular plates subjected to localised blast loading - Importance in numerical simulations. *International Journal of Impact Engineering*, 2009. 36(1): p. 40–52.

[19] Langdon, G. S., et al., Behaviour of fibre-metal laminates subjected to localised blast loading – Part I: Experimental observations. *International Journal of Impact Engineering*, 2007. 34(7): p. 1202–1222.

[20] Lemanski, S. L., et al., Behaviour of fibre metal laminates subjected to localised blast loading - Part II: Quantitative analysis. *International Journal of Impact Engineering*, 2007. 34(7): p. 1223–1245.

[21] Karagiozova, D., et al., Simulation of the response of fibre-metal laminates to localised blast loading. *International Journal of Impact Engineering*, 2010. 37(6): p. 766–782.

[22] Langdon, G. S., et al., Failure characterisation of blast-loaded fibre-metal laminate panels based on aluminium and glass-fibre reinforced polypropylene. *Composites Science and Technology*, 2007. 67(7–8): p. 1385–1405.

[23] Lemanski, S. L., et al., Understanding the behaviour of fibre metal laminates subjected to localised blast loading. *Composite Structures*, 2006. 76(1–2): p. 82–87.

[24] Langdon, G. S., W. J. Cantwell and G. N. Nurick, Localised blast loading of fibre-metal laminates with a polyamide matrix. *Composites Part B: Engineering*, 2007. 38(7–8): p. 902–913.

[25] Langdon, G. S., et al., Response of GLARE panels to blast loading. *Engineering Structures*, 2009. 31(12): p. 3116–3120.

[26] Johnson, W., *Impact strength of materials*. 1972, London: Edward Arnold (Publishers) Limited.

[27] Zhao, Y. -P., Suggestion of a new dimensionless number for dynamic plastic response of beams and plates. *Archive of Applied Mechanics* (Ingenieur Archiv), 1998. 68(7–8): p. 524–538.

[28] Li, Q. M. and N. Jones, On dimensionless numbers for dynamic plastic response of structural members. *Archive of Applied Mechanics* (Ingenieur Archiv), 2000. 70: p. 245–254.

[29] Li, Q. M. and H. Meng, Pulse loading shape effects on pressure-impulse diagram of an elastic-plastic, single-degree-of-freedom structural model. *International Journal of Mechanical Sciences*, 2002. 44(9): p. 1985–1998.

[30] Fallah, A. S. and L. A. Louca, Pressure-impulse diagrams for elastic-plastic-hardening and softening single-degree-of-freedom models subjected to blast loading. *International Journal of Impact Engineering*, 2007. 34(4): p. 823–842.

[31] Langdon, G. S., et al., The air-blast response of sandwich panels with composite face sheets and polymer foam cores: Experiments and predictions. *International Journal of Impact Engineering*, 2013. 54: p. 64–82.

[32] Buckingham, E., On physically similar systems; Illustrations of the use of dimensional equations. *Physical Review*, 1914. 4(4): p. 345.

[33] Hopkinson, B., *British Ordnance Board Minutes*, 1915, British Ordnance Board.

[34] Cranz, C., Lehrbuch der Ballistic. 1926, Berlin: Springer.

[35] ANSYS AUTODYN, 2010.

[36] MATLAB R2010b, 2010, The MathWorks.

[37] Langdon, G. S., et al., The response of sandwich structures with composite face sheets and polymer foam cores to air-blast loading: Preliminary experiments. *Engineering Structures*, 2012. 36(0): p. 104–112.

[38] SSAB. Armox 370T Class 1 Protection Plate. 2012 08/11/12]; Available from: http://www.ssab.com/Global/ARMOX/Datasheets/en/371_ARMOX_370T_Class1_UK_Data%20Sheet.pdf.

[39] Nurick, G. N. and J. B. Martin, Deformation of thin plates subjected to impulsive loading–A review: Part II: Experimental studies. *International Journal of Impact Engineering*, 1989. 8(2): p. 171–186.

[40] Nurick, G. N. and G. C. Shave, The deformation and tearing of thin square plates subjected to impulsive loads – An experimental study. *International Journal of Impact Engineering*, 1996. 18(1): p. 99–116.

[41] Chung Kim Yuen, S., et al., Response of V-shape plates to localised blast load: Experiments and numerical simulation. *International Journal of Impact Engineering*, 2012. 46: p. 97–109.

[42] ABAQUS/CAE, 2009, *Dassault Systemes*.

[43] Micallef, K., et al. The dynamic performance of simply-supported rigid-plastic circular steel plates subjected to localised blast loading. *International Journal of Mechanical Sciences* 65.1 (2012): 177–191.

[44] Fallah, A. S., et al. Dynamic response of Dyneema® HB26 plates to localised blast loading. *International Journal of Impact Engineering* 73 (2014): 91–100.

[45] Micallef, K., et al. Dynamic Performance of Simply Supported Rigid Plastic Circular Thick Steel Plates Subjected to Localized Blast Loading. *Journal of Engineering Mechanics* 140.1 (2013): 159–171.

[46] Micallef, K., et al. On the dynamic plastic response of steel membranes subjected to localised blast loading. *In International Journal of Impact Engineering*.